Nano Research 2015, 8(5): 1648–1658
DOI 10.1007/s12274-014-0654-1
Research Article
ISSN 1998-0124
CN 11-5974/O4

Visible-light-driven enhanced antibacterial and biofilm elimination activity of graphitic carbon nitride by embedded Ag nanoparticles

Wei Bing[1,2], Zhaowei Chen[1], Hanjun Sun[1], Peng Shi[1], Nao Gao[1], Jinsong Ren[1], and Xiaogang Qu[1] (✉)

[1] *Laboratory of Chemical Biology, Division of Biological Inorganic Chemistry, State Key Laboratory of Rare Earth Resource Utilization, Changchun Institute of Applied Chemistry, University of Chinese Academy of Sciences, Chinese Academy of Sciences, Changchun, Jilin 130022, China*

[2] *College of Life Science, Jilin University, Changchun, Jilin 130012, China*

Received: 11 Octobrt 2014
Revised: 17 November 2014
Accepted: 21 November 2014

KEYWORDS
graphitic carbon nitride, $Ag/g\text{-}C_3N_4$ nanohybrids, antibacterial platform, reactive oxygen species (ROS), biofilm

ABSTRACT

Semiconductor nanomaterials with photocatalytic activity have potential for many applications. An effective way of promoting photocatalytic activity is depositing noble metal nanoparticles (NPs) on a semiconductor, since the noble metal NPs act as excellent electron acceptors which inhibit the quick recombination of the photoexcited electron–hole pairs and thereby enhance the generation of reactive oxygen species (ROS). Herein, a highly effective platform, graphitic carbon nitride ($g\text{-}C_3N_4$) nanosheets with embedded Ag nanoparticles ($Ag/g\text{-}C_3N_4$), was synthesized by a facile route. Under visible light irradiation, the ROS production of $Ag/g\text{-}C_3N_4$ nanohybrids was greatly improved compared with pristine $g\text{-}C_3N_4$ nanosheets, and moreover, the nanohybrids showed enhanced antibacterial efficacy and ability to disperse bacterial biofilms. We demonstrate for the first time that the $Ag/g\text{-}C_3N_4$ nanohybrids are efficient bactericidal agents under visible light irradiation, and can also provide a new way for biofilm elimination. The enhanced antibacterial properties and biofilm-disrupting ability of $Ag/g\text{-}C_3N_4$ nanohybrids may offer many biomedical applications.

1 Introduction

Infectious diseases induced by bacteria are inevitable in modern medicine, and this continues to be one of the greatest health problems worldwide [1]. Biofilms are sessile communities of microbial cells [2], which usually grow on biomaterial implants and cause significant problems of medical infection, and thus deserve particular attention [3]. Antibiotics are extensively used in our daily life and have saved the lives of millions of people [4]. However, bacteria have evolved several resistance mechanisms against antibiotics. Meanwhile, biofilms are also hard to eradicate with antibiotics due to the protection offered by the mode

Address correspondence to xqu@ciac.ac.cn

of growth [1], thus making their treatment extremely difficult [4]. More recently, antibacterial nanomaterials have been shown to directly destroy bacteria without targeting a very specific step in their metabolic pathways—as most antibiotics do—and thus there may be less opportunity for mutation or other alterations which can impart resistance [5]. In this respect, several kinds of nanomaterials have been developed as functional antimicrobials, including carbon-based, metallic, and semiconductor materials. Among those, some semiconductor materials have been proven to be effective and eco-friendly antibacterial agents. With the activation of ultraviolet (UV) light irradiation, semiconductor photocatalysts, such as TiO_2 and ZnO, have been used as antimicrobials with activation by UV light [6, 7]. However, the UV light required for the excitation occupies only 4% of the incoming solar spectrum, and it is harmful to organisms [8]. Compared with UV light, visible light is abundant in nature and less harmful to living organisms. Hence, developing new compositions absorbing visible light irradiation is necessary for more efficient utilization of solar energy.

Recently, graphitic carbon nitride (g-C_3N_4) has been suggested as an efficient photocatalyst for cancer therapy [9] and photodegradation of organic pollutants [10] based on its ability to produce electron–hole pairs upon visible illumination and thereby create highly reactive oxygen species (ROS), but it has been only rarely used as an antibacterial agent [8, 11]. This might be due to the limited ROS generation ability of pristine g-C_3N_4. However, noble metal nanoparticles (NPs) can increase photoenergy conversion efficiency of semiconductors by facilitating creation of electron–hole pairs and extending spectral absorption [12–14]. Thus, it has been reported that the photcatalytic activity of semiconductors can be enhanced by embedding noble metal NPs [15–17]. Of particular interest, the photocatalytic activity of g-C_3N_4 could also be significantly enhanced by embedded noble metal NPs [18–20], since the noble metal NPs can act as excellent electron acceptors to inhibit the quick recombination of the photoexcited electron–hole pairs and so enhance the generation of ROS.

Therefore, inspired by the aforementioned mechanism, we established an effective platform based on the g-C_3N_4 nanosheets with embedded AgNPs (Ag/g-C_3N_4 nanohybrids) for enhanced visible-driven antibacterial activity and dispersal of biofilms (Scheme 1). The ROS production of Ag/g-C_3N_4 nanohybrids was much more effective than g-C_3N_4 nanosheets alone under visible illumination. In addition, under visible light illumination, it was found that Ag/g-C_3N_4 nanohybrids could degrade proteins, exopolysaccharides and nucleic acids, which are the main components of biofilms [2]. Hence, the nanohybrids of Ag/g-C_3N_4 were efficient bactericidal agents for both gram-negative (G^-) *Escherichia coli* (*E. coli*) and gram-positive (G^+) *Staphylococcus aureus* (*S. aureus*) under visible light irradiation. Moreover, Ag/g-C_3N_4 nanohybrids constitute a promising alternative for the treatment of refractory biofilms, a much more difficult medical challenge.

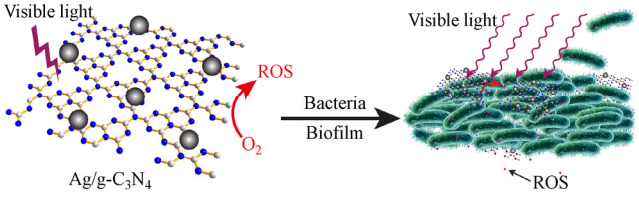

Scheme 1 Schematic diagrams showing the mechanism responsible for the enhanced antibacterial and biofilm elimination of Ag/g-C_3N_4 under visible light irradiation.

2 Experimental

2.1 Preparation of ultrathin g-C_3N_4 nanosheets

The bulk g-C_3N_4 was prepared by direct polymerization of melamine at high temperature. In detail, melamine was placed in an alumina crucible with a cover and then heated at 600 °C for 2 h with a ramp rate of about 3 °C·min^{-1} for both the heating and cooling processes. The obtained yellow product was g-C_3N_4 powder [9, 21]. Ultrathin g-C_3N_4 nanosheets were obtained by liquid exfoliation of as-prepared bulk g-C_3N_4 in water. In detail, 100 mg of bulk g-C_3N_4 powder was dispersed in 100 mL of 5 M HNO_3 and then refluxed for about 16 h. The initially formed white suspension was then centrifuged at about 5,000 rpm to remove the residual unexfoliated g-C_3N_4 nanoparticles before use [9, 21].

2.2 Preparation of Ag/g-C_3N_4 nanohybrids

Sixty milligrams of as-prepared g-C_3N_4 nanosheets was dispersed in water (2 mL) by mild sonication for

2 min. $AgNO_3$ solution (0.5 mL; 2 mM) was added to this suspension and stirred in the dark for 1 h, followed by adding $NaBH_4$ (0.2 mL; 1 mM). The resulting mixture was stirred under visible light for 1 h and washed thoroughly with distilled water and finally dried in a vacuum oven at 60 ℃ for further use.

2.3 Bacterial culture and antibacterial experiments

Monocolonies of *E. coli* and *S. aureus* on solid Luria–Bertani (LB) agar plates were transferred to 20 mL of liquid LB culture medium and grown at 37 ℃ for 12 h under 180 rpm rotation. Then the bacteria were diluted with broth to 10^6 cfu·mL^{-1} [22]. In all experiments, the concentrations of bacteria were determined by measuring the optical density at 600 nm (OD_{600nm}). An AgNPs+g-C_3N_4 mixture with same Ag content as Ag/g-C_3N_4 nanohybrids was used as a control. The as-prepared bacteria solution (500 μL) was mixed with pristine g-C_3N_4 or Ag/g-C_3N_4 nanohybrids for 30 min under visible light illumination. The reaction temperature was maintained at 25 ℃ and the reaction mixture was stirred with a magnetic stirrer throughout the experiment. Then, the solution was placed on a solid medium by the spread plate method and cultured at 37 ℃ for 24 h. Control experiments were performed in parallel without g-C_3N_4 or Ag/g-C_3N_4.

2.4 Biofilm formation by *S. aureus*

To develop biofilms, 10 μL of stationary growth phase *S. aureus* bacterial culture (requiring about 12 h growth at 37 ℃ in LB medium) and 990 μL TSB medium (3%, containing 1% glucose) were added into 24-well microtiter plates [22]. The microtiter plates were then incubated in air at 37 ℃. The medium was discarded and fresh medium added every 24 h. After 48 h, each well was washed with PBS buffer under aseptic condition to eliminate medium and unbound bacteria [22, 23]. Biofilms could be observed on the bottom of the wells.

2.5 Destruction of *S. aureus* biofilm by Ag/g-C_3N_4 nanohybrids

The obtained biofilms of *S. aureus* were treated with both pristine g-C_3N_4 and Ag/g-C_3N_4 nanohybrids for 3 h under visible light illumination in biofilm minimal media (TSB medium). The remaining biofilms were washed once with PBS (1.0 mL), before adding crystal violet stain (1.0 mL; 0.2% crystal violet, 1.9% ethanol and 0.08% ammonium oxalate in PBS). The plates were incubated on the bench for 30 min before washing the wells with PBS (2 × 1.0 mL). The amount of remaining crystal violet stained biofilms were quantified by adding 100% ethanol (1.0 mL) and measuring OD_{590nm} of the homogenized suspension [24, 25]. The same 48 h old biofilms under visible light illumination for 3 h in biofilm minimal media (TSB medium) were measured as a control.

2.6 Detection of photogenerated reactive oxygen species

The ROS performance of the prepared samples was evaluated by measuring the degradation of 2′,7′-dichlorofluorescein diacetate (DCFH-DA) under visible light irradiation. A 300 Watt quartz halogen lamp was used as the visible light source. The dye is a nonfluorescent compound which readily diffuses into water and reacts with reactive oxygen radicals. The product dichlorofluorescein (DCF) is a fluorophore with excitation and emission wavelengths of 485 and 525 nm, respectively and the fluorescence can be quantitatively correlated with the amount of ROS. For a typical test, DCFH-DA solution was added to the composites, and the mixtures were incubated under visible irradiation for 10 min. The reaction temperature was maintained at 25 ℃ while the reaction mixture was stirred with a magnetic stirrer throughout the experiment [26].

2.7 Cleavage of polysaccharides, nucleic acids and proteins

Chitosan hydrogels were prepared with glutaraldehyde crosslinking. Chitosan at 1% was dissolved in 500 μL of NaAc (0.1 M, pH 4.5) and incubated with 0.2% glutaraldehyde at 25 ℃ for 1 h [3]. Then 500 μL of g-C_3N_4 or Ag/g-C_3N_4 were added to cover these gels in the glass vial and incubated under visible light illumination for 3 h. The supernatant was discarded and the remaining gels were rinsed three times with water. Contact with filter paper for 1 h was used to remove water and uncrosslinked chitosan, and the

mass of the remaining gel was recorded. The volume of remaining gel was visualized after inversion in the glass vial. To investigate the degradation of DNA, *S. aureus* genome DNA was extracted with a bacteria genome DNA kit, and nucleic acid cleavage assays were performed in 50 μL of g-C_3N_4 or Ag/g-C_3N_4 under visible light illumination for 3 h. In these later experiments, nucleic acid cleavage products were identified with agarose gel electrophoresis and ethidium bromide staining. To obtain whole-cell proteins, *S. aureus* cells were disrupted by sonication, and soluble supernatant was obtained by centrifugation (10,000 rpm for 15 min). Protein cleavage assays were performed in 50 μL of g-C_3N_4 or Ag/g-C_3N_4 under visible light illumination for 3 h prior to separation with SDS-PAGE and Coomassie blue R-250 staining.

3 Results and discussion

The g-C_3N_4 nanosheets were synthesized from melamine powder according to a previously reported method with some modification [21]. The morphology of the g-C_3N_4 nanosheets was first characterized by transmission electron microscopy (TEM) and atomic force microscopy (AFM). As shown in Figs. S1 and S2 (in the Electronic Supplementary Material (ESM)), the prepared g-C_3N_4 was well dispersed as ultrathin nanosheets with a lateral size ranging from 100 to 150 nm and an average height of ca. 2.8 nm. Subsequently, Ag/g-C_3N_4 nanohybrids were synthesized via a conventional solution impregnation method [27]. AgNPs with diameters in the range 5–30 nm were formed *in situ* on the g-C_3N_4 nanosheets (Fig. 1(a)) and the average size was 6.2 nm (Fig. S3, in the ESM). A high-resolution TEM (HRTEM) image taken from the NPs (Fig. 1(b)) revealed clear lattice fringes with an interplane distance of 0.236 nm corresponding to the (111) lattice space of metallic Ag, confirming the NPs were indeed AgNPs.

The X-ray diffraction (XRD) pattern further supported the formation of Ag/g-C_3N_4 nanohybrids (Fig. 1(c)). The diffraction peak at 27.4° is characteristic of the stacking of the conjugated aromatic system in graphitic materials and can be indexed as the (002) peak of g-C_3N_4. After deposition of Ag, the typical peaks of Ag (111, 200, 220, and 311) indicate the formation of crystalline AgNPs, and the predominantly exposed faces were consistent with the HRTEM observation. X-ray photoelectron spectroscopy (XPS) studies were carried out to determine the surface composition of the Ag/g-C_3N_4 nanohybrids and the results are shown in Fig. 1(d). The characteristic binding energies of Ag $3d_{5/2}$ (368.2 eV) and Ag $3d_{3/2}$ (374.2 eV) correspond to the literature values for metallic Ag^0 species (Fig. S4, in the ESM) [28, 29].

Optical absorption spectra of the as-prepared g-C_3N_4 nanosheets and Ag/g-C_3N_4 nanohybrids were also investigated. (Fig. S5, in the ESM). Unlike g-C_3N_4, the Ag/g-C_3N_4 showed an absorption peak around 400 nm, which can be attributed to the absorption of AgNPs. The plasmon resonance absorption of Ag offers the possibility of highly efficient utilization of visible light [17] and enhancement of the generation of ROS by Ag/g-C_3N_4 nanohybrids [6]. Figure 1(e) shows the photoluminescence (PL) spectra of g-C_3N_4 and Ag/g-C_3N_4 samples excited by 325 nm radiation. The PL intensity of the Ag/g-C_3N_4 nanohybrids was lower than that of g-C_3N_4 nanosheets, which suggests a reduced recombination probability of photogenerated charge carriers in the Ag/g-C_3N_4 nanohybrids in comparison to the pristine g-C_3N_4 [30]. In addition, the results of Fourier transform infrared spectroscopy (FT-IR) are presented in Fig. 1(f). The broad bands at 3,176 cm^{-1} and 1,200–1,700 cm^{-1} can be attributed to the stretching vibrations of N–H groups and aromatic C–N heterocycles, respectively. The vibration at 808 cm^{-1} can be assigned to the characteristic breathing mode of triazine units in g-C_3N_4 [31, 32]. In the case of Ag/g-C_3N_4 nanohybrids, the intensities of all the characteristic bands of g-C_3N_4 were decreased to some extent compared to those of the pristine g-C_3N_4. This can be attributed to the insertion of Ag atoms into the g-C_3N_4 matrix and formation of new Ag–N bonds. The PL and FT-IR results are both indicative of tight covalent binding between AgNPs and g-C_3N_4 nanosheets. According to inductively coupled plasma optical emission results, the weight content of Ag in the Ag/g-C_3N_4 nanohybrids was 0.095 g/g.

To examine the antibacterial activity of Ag/g-C_3N_4 nanohybrids, we first tested the growth kinetics of G^- and G^+ bacteria. *E. coli* and *S. aureus* were chosen as models to evaluate the bactericidal performance and

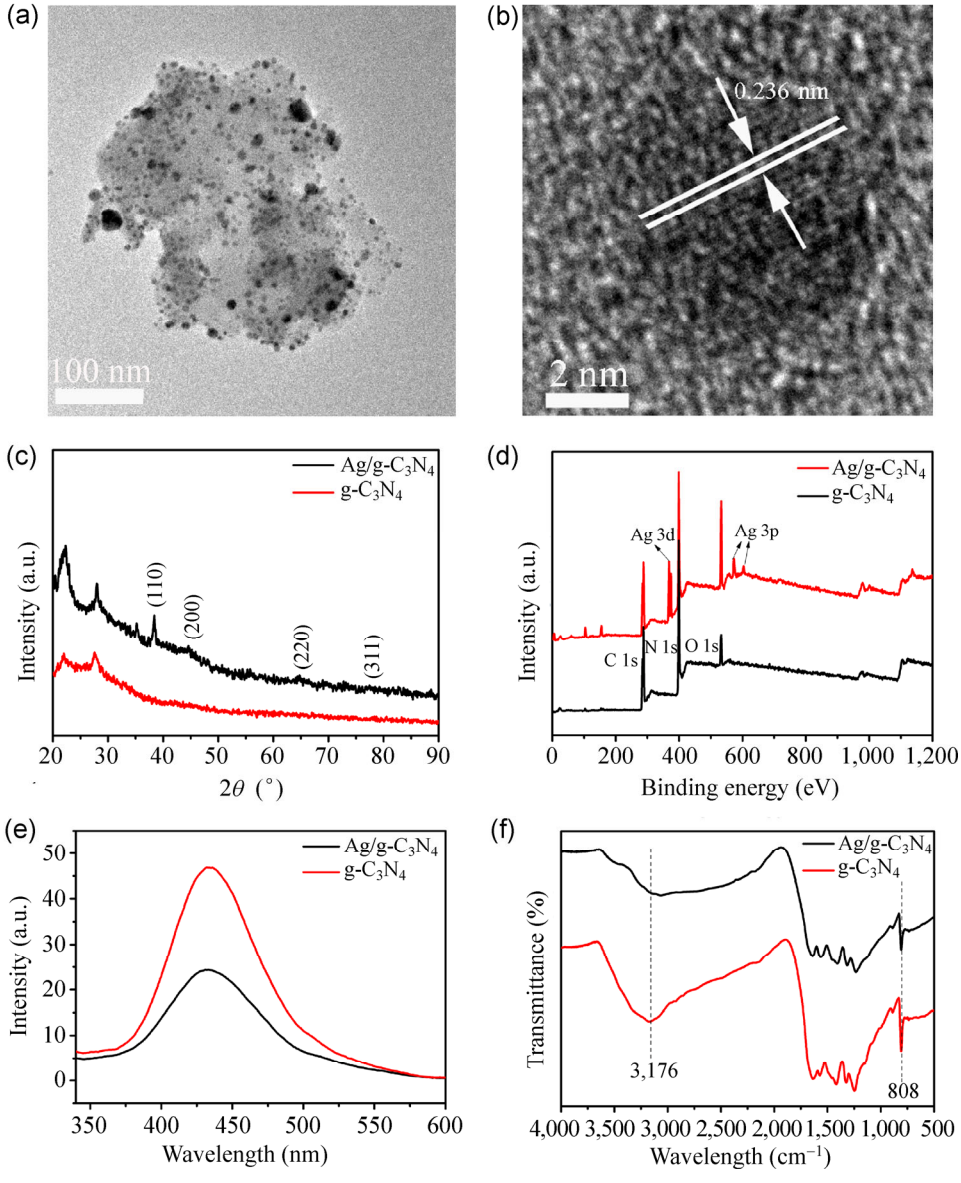

Figure 1 (a) TEM images of Ag/g-C_3N_4 and (b) HRTEM image of the composite. (c) XRD patterns of g-C_3N_4 and Ag/g-C_3N_4. (d) XPS analysis surveys of g-C_3N_4 and Ag/g-C_3N_4. (e) Photoluminescence spectra and (f) FT-IR spectra of g-C_3N_4 and Ag/g-C_3N_4.

mechanism of disinfection. As a control, AgNPs with similar size were prepared (Figs. S6(a) and S6(b), in the ESM) [33]. We compared the bactericidal efficiency of Ag/g-C_3N_4 nanohybrids, g-C_3N_4, and physically mixed AgNPs and g-C_3N_4 (AgNPs+g-C_3N_4). The growth rates of bacterium *E. coli* and *S. aureus* were evaluated in a LB culture medium, and the results are determined by OD measurements. The agents (Ag/g-C_3N_4 nanohybrids, AgNPs+g-C_3N_4, pristine g-C_3N_4) with different concentrations were added to LB medium and incubated for 30 min under visible light irradiation. For the physically mixed AgNPs+g-C_3N_4, the mass ratio of AgNPs to g-C_3N_4 was adjusted to 1:10, consistent with that of Ag/g-C_3N_4 nanohybrids. The corresponding activities are summarized in Fig. 2. The results demonstrated that after 12 h culture, for *E. coli* and *S. aureus*, the Ag/g-C_3N_4 nanohybrids exhibited strongest antibacterial activity (Figs. 2(b) and 2(d)). Based on the concentration of AgNPs in Ag/g-C_3N_4 nanohybrids, the antibacterial activity of AgNPs alone at the same concentration was explored as well. As displayed in Fig. S7 (in the ESM), it had

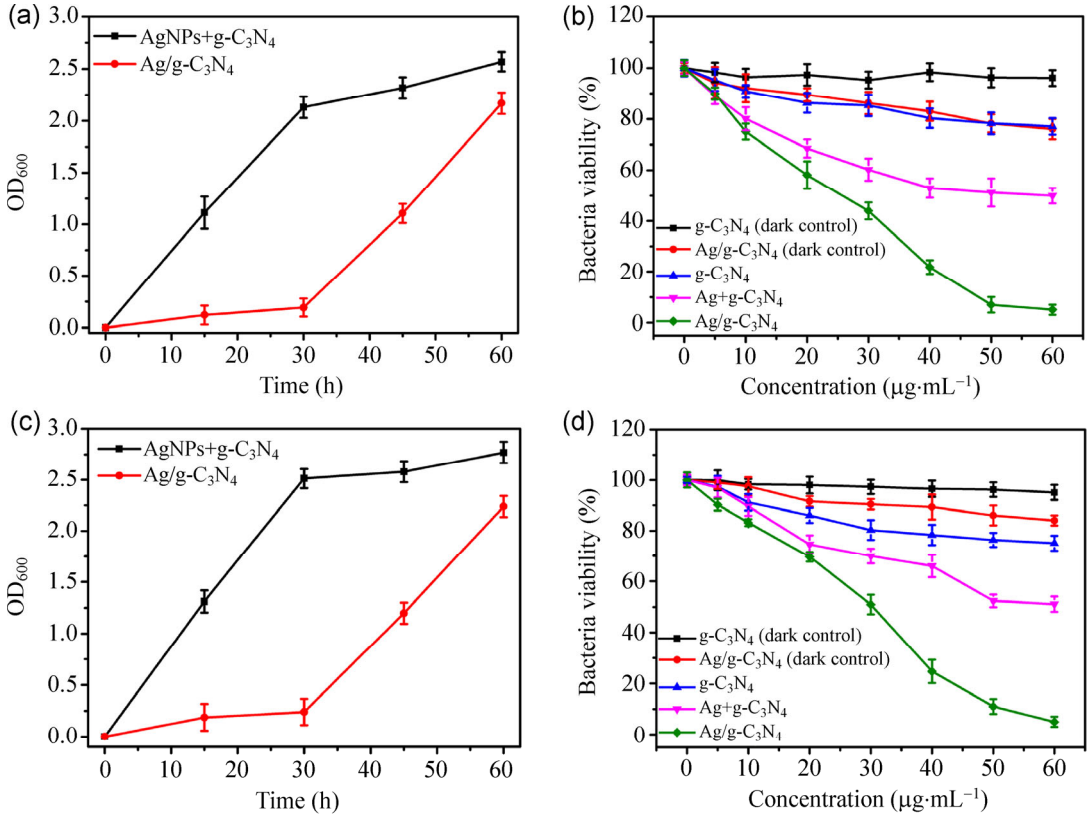

Figure 2 The growth curves of (a) *E. coli* and (c) *S. aureus* treated with 50 μg·mL^{-1} of AgNPs+g-C_3N_4 or Ag/g-C_3N_4 under visible light irradiation for 30 min. The bacterial viability of (b) *E. coli* and (d) *S. aureus* incubated with different concentrations of g-C_3N_4, AgNPs+g-C_3N_4 or Ag/g-C_3N_4 under visible light irradiation for 30 min and a dark control.

minimal antibacterial activity. Furthermore, Ag/g-C_3N_4 showed longer term efficacy than AgNPs+g-C_3N_4 (Figs. 2(a) and 2(c)). For the Ag/g-C_3N_4 nanohybrids, the inactivation efficiency could nearly reach 100% when the concentration was 50 and 60 μg·mL^{-1} for *E. coli* and *S. aureus*, respectively. Moreover, Ag/g-C_3N_4 effectively inhibited the growth of *E. coli*, and the antibacterial activity was enhanced with increasing visible light irradiation time. According to Fig. S8 (in the ESM), *E. coli* was almost completely killed within 60 min using Ag/g-C_3N_4 nanohybrids at a concentration of 30 μg·mL^{-1} under visible light irradiation. These results indicate that the Ag/g-C_3N_4 nanohybrids are an effective and rapid bactericidal agent even at low concentrations and with short illumination times. We also studied the effect of the content of AgNPs in the Ag/g-C_3N_4 nanohybrids on the antibacterial activity (Fig. S9, in the ESM). When the mass ratio of AgNPs to g-C_3N_4 was 1:10, the antibacterial viability was improved significantly compared with that for 1:20. However, if the mass ratio of AgNPs to g-C_3N_4 was increased to 1:5, the antibacterial ability was not significantly further enhanced.

Further tests of the viability were conducted by observing the number of colony-forming units on LB agar plates. Figure 3 shows the formation of bacterial colonies on LB agar treated with Ag/g-C_3N_4, AgNPs+g-C_3N_4 and g-C_3N_4 after 24 h cultivation. Compared with the control, a remarkable difference was observed in the plates containing Ag/g-C_3N_4 (50 μg·mL^{-1}) after visible light irradiation. Colony formation was almost completely prevented when bacteria were incubated on Ag/g-C_3N_4 stained LB-agar, while a large number of colonies could be seen on LB agar stained with either AgNPs+g-C_3N_4 or g-C_3N_4 alone. These results confirm that Ag/g-C_3N_4 exhibited the best inhibition ability toward both G^- and G^+ bacteria. The result of a control experiment indicated that visible light alone caused no photolysis of bacterial cells (Fig. 3). Furthermore, the effects on *E. coli* and *S. aureus*

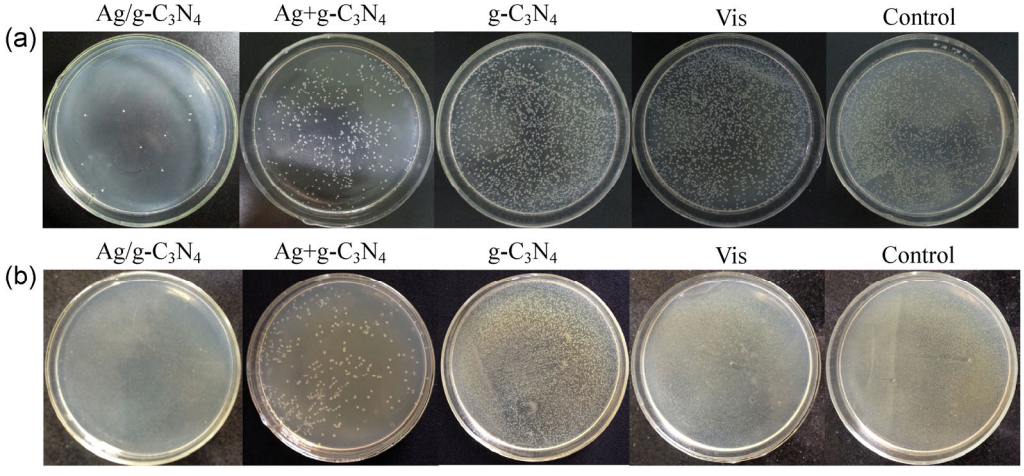

Figure 3 The plate samples showing colonies of (a) *E. coli* and (b) *S. aureus* incubated with g-C_3N_4, AgNPs+g-C_3N_4 or Ag/g-C_3N_4 under visible light illumination for 30 min. Vis: visible light illumination for 30 min only; control: dark control.

treated with Ag/g-C_3N_4 (30 μg·mL^{-1}) under visible light illumination for 30 min were studied by scanning electron microscopy (SEM). The SEM images indicated cell membrane disruption or crimpling (Fig. 4). This suggests that cell membrane damage was caused by the ROS generated by Ag/g-C_3N_4 nanohybrids and the released silver ions [34, 35].

Compared with bacteria, biofilms are more difficult to eradicate due to the protection offered by the matrix formed during biofilm growth [1, 2]. *S. aureus* is the most often isolated pathogen from infected biomaterial implant surfaces, and can develop into biofilms on biomaterial implants. These are detected in approximately 23% of infections connected with prosthetic joints [1] and can cause serious infections such as pulmonitis, ichorrhemia or joint infections [36]. Therefore, the effect of the Ag/g-C_3N_4 nanohybrid antibacterial agent on the destruction of *S. aureus* biofilms was also explored. In this experiment, treatment with g-C_3N_4 nanosheets and Ag/g-C_3N_4 nanohybrids

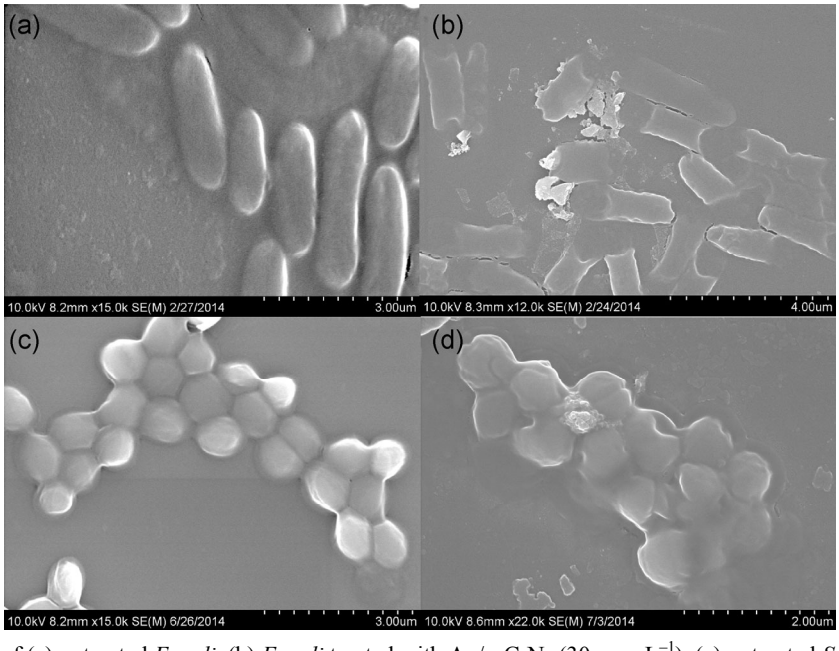

Figure 4 SEM images of (a) untreated *E. coli*, (b) *E. coli* treated with Ag/g-C_3N_4 (30 μg·mL^{-1}), (c) untreated *S. aureus* and (d) *S. aureus* incubated with Ag/g-C_3N_4 (30 μg·mL^{-1}) under visible light illumination for 30 min. All incubations were at 37 ˚C, overnight.

in the concentration range of 0–200 μg·mL^{-1} was carried out under visible light illumination for 3 h in Tryptone Soy Broth (TSB) medium. The results revealed that biofilms showed a rapid and dose-dependent dispersal response to Ag/g-C_3N_4 nanohybrids, removing 70% of the biofilm mass after treatment with 200 μg·mL^{-1} Ag/g-C_3N_4 nanohybrids (Figs. 5(c) and 5(d)). In contrast, wells treated with pristine g-C_3N_4 still showed clear biofilm bands even at a concentration of 200 μg·mL^{-1} (Figs. 5(a) and 5(b)). The biofilm mass was quantified by the crystal violet staining method [24, 25]. The results demonstrated that the Ag/g-C_3N_4 nanohybrids are effective for biofilm elimination. Moreover, treatment with Ag/g-C_3N_4 nanohybrids could also cause bacterial death in the residual biofilms (Fig. S10, in the ESM).

Based on the above results, ROS generation by the Ag/g-C_3N_4 nanohybrids, AgNPs+g-C_3N_4 and pristine g-C_3N_4 were investigated and the results are shown in Fig. 6. The ROS monitoring was achieved using DCFH-DA, a nonfluorescent compound which readily diffuses into water and reacts with ROS [26]. The generated DCF is a fluorophore with excitation and emission wavelengths of 485 and 525 nm, respectively. The fluorescence intensity of DCF can be correlated with the amount of ROS. In a typical test, DCFH-DA solution was added to the composites, and the mixtures were incubated under visible light irradiation for 10 min. The extent of ROS formation with Ag/g-C_3N_4 nanohybrids was significantly higher than with AgNPs+g-C_3N_4 or pristine g-C_3N_4 under visible light irradiation (Fig. 6). This suggests that visible light irradiation of g-C_3N_4 nanosheets generated conduction band electrons (e^-) and valence band holes (h^+), and the embedded AgNPs acted as electron traps to facilitate the separation of photogenerated electron–hole pairs and promoted the interfacial electron transfer process. Furthermore, the Ag/g-C_3N_4 nanohybrids increased the efficiency of charge carrier separation, extended the range of light absorption and facilitated the creation of electron–hole pairs [11, 12]. The increased generation of ROS may therefore be the dominant mechanism by which Ag/g-C_3N_4 nanohybrids have an enhanced antibacterial activity and improved elimination of biofilms when compared with the pristine g-C_3N_4 nanosheets.

The mechanism of the destruction of the *S. aureus* biofilms by Ag/g-C_3N_4 nanohybrids was also explored. As demonstrated by the DCFH-DA reaction discussed above, the Ag/g-C_3N_4 nanohybrids showed very high ROS generation ability (Fig. 6). We then tested whether the Ag/g-C_3N_4 nanohybrids could degrade each of the three major components of the biofilms. Polysaccharides are the major component in a biofilm matrix [3]. We chose chitosan as a model polysaccharide, and tested the effect of Ag/g-C_3N_4 nanohybrids

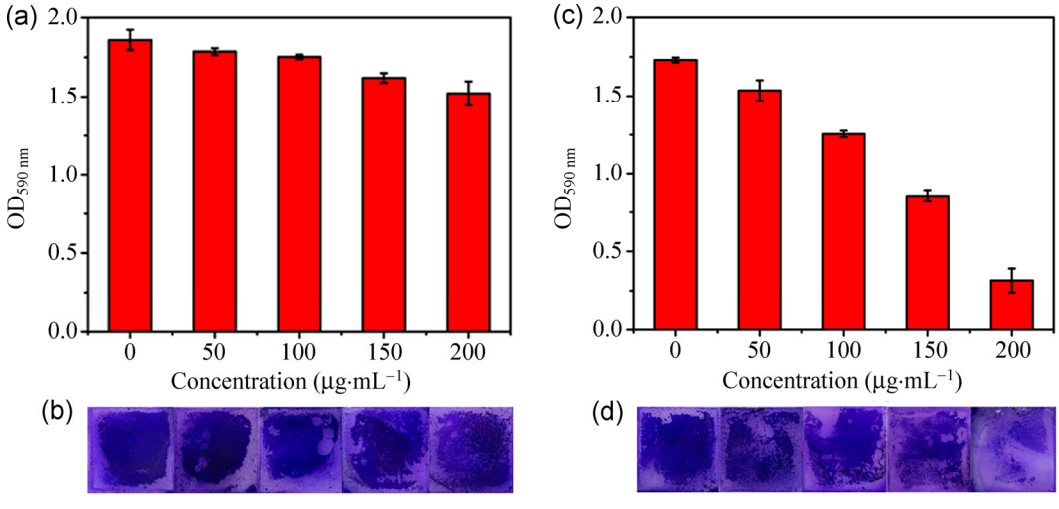

Figure 5 The efficacy of (a) and (b) g-C_3N_4 nanosheets and (c) and (d) Ag/g-C_3N_4 nanohybrids on the elimination of biofilms of *S. aureus* under visible light illumination for 3 h. (a) and (c) The remaining biofilms were quantified by crystal violet staining. The effect of (b) g-C_3N_4 nanosheets and (d) Ag/g-C_3N_4 nanohybrids on the elimination of submerged biofilms. Biofilms were visualized by crystal violet staining.

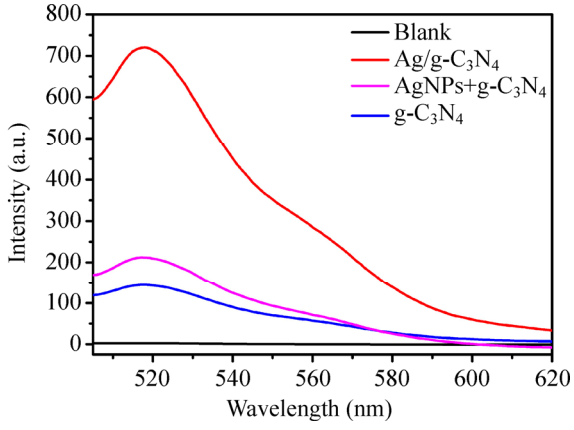

Figure 6 ROS generation by g-C_3N_4, AgNPs+g-C_3N_4 and Ag/g-C_3N_4 at a concentration of 50 μg·mL^{-1} was measured using DCF fluorescence after 10 min visible light irradiation.

and g-C_3N_4 nanosheets on this material. Firstly, chitosan hydrogels were prepared by glutaraldehyde crosslinking in tubes. Then these chitosan gels were incubated with g-C_3N_4 and Ag/g-C_3N_4 nanohybrids under visible light illumination for 3 h. Compared with pristine g-C_3N_4, Ag/g-C_3N_4 nanohybrids had a greater effect in reducing the mass that remained as a gel (Fig. 7).

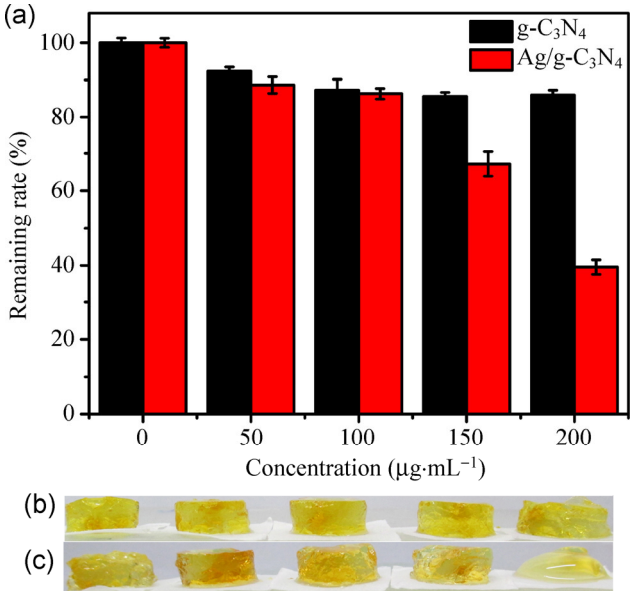

Figure 7 Polysaccharides (chitosan gels) were incubated with g-C_3N_4 and Ag/g-C_3N_4 nanohybrids under visible light illumination for 3 h. The (a) residual ratio of chitosan gels and (b) and (c) pictures of the remaining gels were recorded. Error bars denote standard deviation.

When the concentration of Ag/g-C_3N_4 nanohybrids reached 200 μg·mL^{-1}, the mass of chitosan gel was reduced 60% (Figs. 7(a) and 7(c)). We next investigated the ability of Ag/g-C_3N_4 nanohybrids to degrade whole-cell proteins (Fig. 8(a)) and genome DNA (Fig. 8(b)) under the same reaction conditions. Our results showed that treatment with Ag/g-C_3N_4 nanohybrids at a concentration of 200 μg·mL^{-1} was successful at degrading proteins (Fig. 8(a), lane 3) and nucleic acids (Fig. 8(b), lane 4), but the pristine g-C_3N_4 had no obvious effect. Thus, Ag/g-C_3N_4 nanohybrids showed enhanced cleavage ability of biofilm components such as oligosaccharides, proteins, and nucleic acids. From the above results, we can conclude that Ag/g-C_3N_4 nanohybrids could serve as a platform for the destruction of biofilms since the generated ROS had a higher activity in the oxidation of nucleic acids, proteins

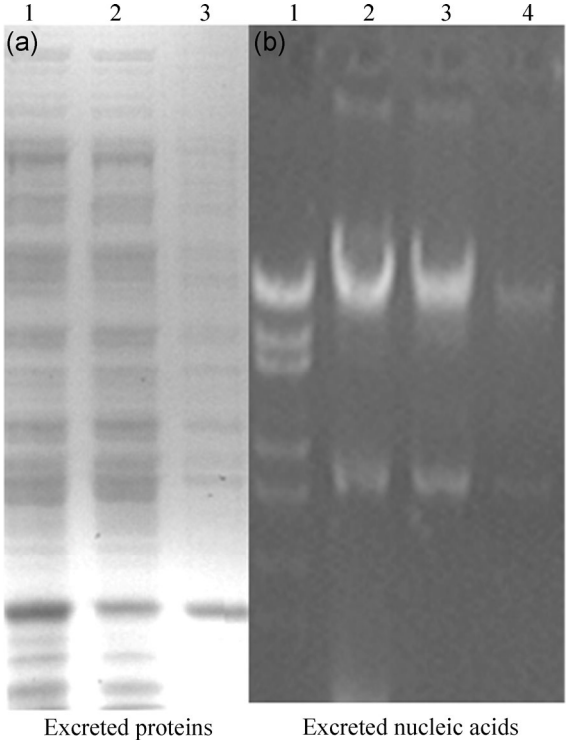

Figure 8 Cleavage of proteins and nucleic acids by g-C_3N_4 nanosheets and Ag/g-C_3N_4 nanohybrids. (a) *S. aureus* lysate was incubated with g-C_3N_4 and Ag/g-C_3N_4 nanohybrids under visible light illumination for 3 h. Lanes 1–3: (1) control with proteins only; (2) g-C_3N_4 (200 μg·mL^{-1}); (3) Ag/g-C_3N_4 (200 μg·mL^{-1}). (b) Genomic DNA was incubated with g-C_3N_4 and Ag/g-C_3N_4 nanohybrids under visible light illumination for 3 h. Lanes 1–4: (1) DNA marker; (2) control with nucleic acids only; (3) g-C_3N_4 (200 μg·mL^{-1}); (4) Ag/g-C_3N_4 (200 μg·mL^{-1}).

and polysaccharides in the matrix of a biofilm, so the Ag/g-C_3N_4 based antibacterial agent can break down the existing biofilm effectively.

4 Conclusion

Ag/g-C_3N_4 nanohybrids exhibit broad antibacterial activity and biofilm-dispersing ability under visible light illumination. Ag/g-C_3N_4 nanohybrids displayed significantly enhanced ROS generation under visible light irradiation. Due to the enhancement of ROS generation, Ag/g-C_3N_4 nanohybrids exhibited improved ability to cleave polysaccharides, nucleic acids and proteins when compared with g-C_3N_4 nanosheets. These results provide an effective way to improve antibacterial and biofilm elimination activity of g-C_3N_4 nanohybrids, and show great potential for biomedical applications.

Acknowledgements

This work was supported by the National Basic Research Program of China (Nos. 2011CB936004 and 2012CB720602) and the National Natural Science Foundation of China (Nos. 21210002, 21431007, 91413111, 21402183).

Electronic Supplementary Material: Supplementary material is available in the online version of this article at http://dx.doi.org/10.1007/s12274-014-0654-1.

References

[1] Subbiandoss, G.; Sharifi, S.; Grijpma, D. W.; Laurent, S.; van der Mei, H. C.; Mahmoudi, M.; Busscher, H. J. Magnetic targeting of surface-modified superparamagnetic iron oxide nanoparticles yields antibacterial efficacy against biofilms of gentamicin-resistant staphylococci. *Acta Biomater.* **2012**, *8*, 2047–2055.

[2] McDougald, D.; Rice, S. A.; Barraud, N.; Steinberg, P. D.; Kjelleberg, S. Should we stay or should we go: Mechanisms and ecological consequences for biofilm dispersal. *Nat. Rev. Micro.* **2012**, *10*, 39–50.

[3] Gao, L. Z; Giglio, K. M.; Nelson, J. L.; Sondermann, H.; Travis, A. J. Ferromagnetic nanoparticles with peroxidase-like activity enhance the cleavage of biological macromolecules for biofilm elimination. *Nanoscale*. **2014**, *6*, 2588–2593.

[4] Rizzello, L.; Pompa, P. P. Nanosilver-based antibacterial drugs and devices: Mechanisms, methodological drawbacks, and guidelines. *Chem. Soc. Reviews*. **2014**, *43*, 1501–1518.

[5] Aruguete, D. M.; Kim, B.; Hochella, M. F.; Ma, Y. J.; Cheng, Y. W.; Hoegh, A.; Liu, J.; Pruden, A. Antimicrobial nanotechnology: Its potential for the effective management of microbial drug resistance and implications for research needs in microbial nanotoxicology. *Environ. Sci.:Processes Impacts.* **2013**, *15*, 93–102.

[6] He, W. W.; Kim, H. K.; Wamer, W. G.; Melka, D.; Callahan J. H.; Yin, J. J. Photogenerated reactive oxygen species and charge carriers in ZnO/Au hybrid nanostructures are correlated with enhanced photocatalytic and antibacterial activity. *J. Am. Chem. Soc.* **2014**, *136*, 750–757.

[7] Zhang, H. J.; Chen, G. H. Potent antibacterial activities of Ag/TiO_2 nanocomposite powders synthesized by a one-pot sol-gel method. *Environ. Sci. Technol.* **2009**, *43*, 2905–2910.

[8] Huang, J. H.; Ho, W.; Wang, X. C. Metal-free disinfection effect induced by graphitic carbon nitride polymers with visible light illumination. *Chem. Commun*. **2014**, *50*, 4338–4340.

[9] Lin, L. S.; Cong, Z. X.; Li, J.; Ke, K. M.; Guo, S. S.; Yang, H. H.; Chen, G. N. Graphitic-phase C_3N_4 nanosheets as efficient photosensitizers and pH-responsive drug nanocarriers for cancer imaging and therapy. *J. Mater. Chem. B*. **2014**, *2*, 1031–1037.

[10] Niu, P.; Zhang, L. L.; Liu, G.; Cheng, H. M. Graphene-like carbon nitride nanosheets for improved photocatalytic activities. *Adv. Funct. Mater.* **2012**, *22*, 4763–4770.

[11] Wang, W. J.; Yu, J. C.; Xia, D. H.; Wong, P. K.; Li, Y. C. Graphene and g-C_3N_4 nanosheets cowrapped elemental α-sulfur as a novel metal-free heterojunction photocatalyst for bacterial inactivation under visible-light. *Environ. Sci. Technol.* **2013**, *47*, 8724–8732.

[12] Atwater, H. A.; Polman, A. Plasmonics for improved photovoltaic devices. *Nat. Mater.* **2010**, *9*, 205–213.

[13] Liu, Z. W.; Hou, W. B.; Pavaskar, P.; Aykol, M.; Cronin, S. B. Plasmon resonant enhancement of photocatalytic water splitting under visible illumination. *Nano Lett*. **2011**, *11*, 1111–1116.

[14] Mubeen, S.; Lee, J.; Singh, N.; Kramer, S.; Stucky G. D.; Moskovits, M. An autonomous photosynthetic device in which all charge carriers derive from surface plasmons. *Nat. Nanotechnol*. **2013**, *8*, 247–251.

[15] Dukovic, G.; Merkle, M. G.; Nelson, J. H.; Hughes S. M.; Alivisatos, A. P. Photodeposition of Pt on colloidal CdS and CdSe/CdS semiconductor nanostructures. *Adv. Mater*. **2008**, *20*, 4306–4311.

[16] Fan, F. R.; Ding, Y.; Liu, D. Y.; Tian, Z. Q.; Wang, Z. L. Facet-selective epitaxial growth of heterogeneous nanostructures of semiconductor and metal: ZnO nanorods on Ag nanocrystals. *J. Am. Chem. Soc*. **2009**, *131*, 12036–12037.

[17] Zhou, W.; Li, T.; Wang, J. Q.; Qu, Y.; Pan, K.; Xie, Y.; Tian, G. H.; Wang, L.; Ren, Z. Y.; Jiang, B. J. et al. Composites of small Ag clusters confined in the channels of well-ordered mesoporous anatase TiO_2 and their excellent solar-light-driven photocatalytic performance. *Nano. Res.* **2014**, *7*, 731–742.

[18] Bu, Y. Y.; Chen, Z. Y.; Li, W. B. Using electrochemical methods to study the promotion mechanism of the photoelectric conversion performance of Ag-modified mesoporous g-C_3N_4 heterojunction material. *Appl. Catal. B-Environ.* **2014**, *144*, 622–630.

[19] Xie, F.; Pang, J. S.; Centeno, A.; Ryan, M. P.; Riley, D. J.; Alford, N. M. Nanoscale control of Ag nanostructures for plasmonic fluorescence enhancement of near-infrared dyes. *Nano. Res.* **2013**, *6*, 496–510.

[20] Chen, X. F.; Zhang, J. S.; Fu, X. Z.; Antonietti, M.; Wang, X. C. Fe-g-C_3N_4-catalyzed oxidation of benzene to phenol using hydrogen peroxide and visible light. *J. Am. Chem. Soc*. **2009**, *131*, 11658–11659.

[21] Zhang, X. D.; Xie, X.; Wang, H.; Zhang, J. J.; Pan, B. C.; Xie, Y. Enhanced photoresponsive ultrathin graphitic-phase C_3N_4 nanosheets for bioimaging. *J. Am. Chem. Soc*. **2013**, *135*, 18–21.

[22] Sun, H. J.; Gao, N.; Dong, K.; Ren, J. S.; Qu, X. G. Graphene quantum dots-band-aids used for wound disinfection. *ACS Nano.* **2014**, *8*, 6202–6210.

[23] Amorena, B.; Gracia, E.; Monzón, M.; Leiva, J.; Oteiza, C.; Pérez, M.; Alabart, J. L.; Hernández-Yago, J. Antibiotic susceptibility assay for *Staphylococcus aureus* in biofilms developed *in vitro*. *J. Antimicrob. Chemother.* **1999**, *44*, 43–55.

[24] Barraud, N.; Kardak, B. G.; Yepuri, N. R.; Howlin, R. P.; Webb, J. S.; Faust, S. N.; Kjelleberg, S.; Rice, S. A.; Kelso, M. J. Cephalosporin-3'-diazeniumdiolates: Targeted NO-donor prodrugs for dispersing bacterial biofilms. *Angew. Chem.* **2012**, *51*, 9057–9060.

[25] Peeters, E.; Nelis, H. J.; Coenye, T. Comparison of multiple methods for quantification of microbial biofilms grown in microtiter plates. *J. Microbiol. Methods.* **2008**, *72*, 157–165.

[26] Li, M.; Liu, Z.; Ren, J. S.; Qu, X. G. Inhibition of metal-induced amyloid aggregation using light-responsive magnetic nanoparticle prochelator conjugates. *Chem. Sci.* **2012**, *3*, 868–873.

[27] Li, X. H.; Wang X. C.; Antonietti, M. Mesoporous g-C_3N_4 nanorods as multifunctional supports of ultrafine metal nanoparticles: Hydrogen generation from water and reduction of nitrophenol with tandem catalysis in one step. *Chem. Sci*. **2012**, *3*, 2170–2174.

[28] Djokovic, V.; Krsmanovic, R.; Bozanic, D. K.; McPherson, M.; Van Tendeloo, G.; Nair, P. S.; Georges M. K.; Radhakrishnan, T. Adsorption of sulfur onto a surface of silver nanoparticles stabilized with sago starch biopolymer. *Colloid Surface B*. **2009**, *73*, 30–35.

[29] Pang, M. L.; Hu J. Y.; Zeng, H. C. Synthesis, morphological control, and antibacterial properties of hollow/solid Ag_2S/Ag heterodimers. *J. Am. Chem. Soc*. **2010**, *132*, 10771–10785.

[30] Ge, L.; Han, C. C.; Liu, J.; Li, Y. F. Enhanced visible light photocatalytic activity of novel polymeric g-C_3N_4 loaded with Ag nanoparticles. *Appl. Catal. A-Gen*. **2011**, *409*, 215–222.

[31] Li, X. F.; Zhang, J.; Shen, L. H.; Ma, Y. M.; Lei, W. W.; Cui, Q. L.; Zou, G. T. Preparation and characterization of graphitic carbon nitride through pyrolysis of melamine. *Appl. Phys. A-Mater.* **2009**, *94*, 387–392.

[32] Thomas, A.; Fischer, A.; Goettmann, F.; Antonietti, M.; Muller, J. O.; Schlogl, R.; Carlsson, J. M. Graphitic carbon nitride materials: Variation of structure and morphology and their use as metal-free catalysts. *J. Mater. Chem.* **2008**, *18*, 4893–4908.

[33] Doty, R. C.; Tshikhudo, T. R.; Brust M.; Fernig, D. G. Extremely stable water-soluble Ag nanoparticles. *Chem. Mater.* **2005**, *17*, 4630–4635.

[34] Zhu, Z. J.; Su, M.; Ma, L.; Ma, L.; Liu, D. J.; Wang, Z. X. Preparation of graphene oxide–silver nanoparticle nanohybrids with highly antibacterial capability. *Talanta.* **2013**, *117*, 449–455.

[35] Yuan, X.; Setyawati, M. I.; Leong, D. T.; Xie, J. P. Ultrasmall Ag^+-rich nanoclusters as highly efficient nanoreservoirs for bacterial killing. *Nano. Res.* **2014**, *7*, 301–307.

[36] Ashkarran, A. A.; Ghavami, M.; Aghaverdi, H.; Stroeve, P.; Mahmoudi, M. Bacterial effects and protein corona evaluations: Crucial ignored factors in the prediction of bio-efficacy of various forms of silver nanoparticles. *Chem. Res. Toxicol.* **2012**, *25*, 1231–1242.